Enhanced Interactions between Gold and MnO2 Nanowires for Water Oxidation: A Comparison of Different Chemical and Physical Preparation Methods

ARTICLE *in* ACS SUSTAINABLE CHEMISTRY & ENGINEERING · AUGUST 2015

Impact Factor: 4.64 · DOI: 10.1021/acssuschemeng.5b00324

10 AUTHORS, INCLUDING:

Chao Lin
Chinese Academy of Sciences
8 PUBLICATIONS **33** CITATIONS
SEE PROFILE

Yonghui Zhao
Chinese Academy of Sciences
18 PUBLICATIONS **135** CITATIONS
SEE PROFILE

Xiaopeng Li
Chinese Academy of Sciences
35 PUBLICATIONS **143** CITATIONS
SEE PROFILE

Yuhan Sun
Chinese Academy of Sciences
599 PUBLICATIONS **7,500** CITATIONS
SEE PROFILE

ACS Sustainable Chemistry & Engineering

Research Article

pubs.acs.org/journal/ascecg

Enhanced Interactions between Gold and MnO_2 Nanowires for Water Oxidation: A Comparison of Different Chemical and Physical Preparation Methods

Haojie Zhang,[†,‡] Chao Lin,[‡] Fuping Du,[‡] Yonghui Zhao,[‡] Peng Gao,[‡] Hao Chen,[‡] Zheng Jiao,[†] Xiaopeng Li,[*,‡] Tiejun Zhao,[*,‡] and Yuhan Sun[‡,§]

[†]College of Environmental and Chemical Engineering, Shanghai University, Shanghai 200444, China

[‡]CAS Key Laboratory of Low-Carbon Conversion Science and Engineering, Shanghai Advanced Research Institute (SARI), Chinese Academy of Sciences (CAS), Shanghai 201210, China

[§]School of Physical Science and Technology, Shanghai Tech University, Shanghai 201210, China

Supporting Information

ABSTRACT: Oxygen evolution reaction (OER) has been considered as the bottleneck step in water electrolysis to simultaneously produce hydrogen and oxygen. The earth abundant first-row metal oxides such as manganese oxide have been found very active after anchoring nanoparticular noble metals such as Au, Pd and Pt onto its surface. Recent reports have demonstrated that Au can increase the turnover frequency (TOF) of MnO_x more than 10 times for the OER due to the unique local interaction between Au and MnO_x. Here, we conducted a detailed comparative study of different preparation methods on the OER activity of Au/MnO_2 nanocomposites, including physical sputtering (PS), deposition–precipitation with urea (DPU), DP with NaOH (DPN) and deposition–reduction (DR) with $NaBH_4$. Through carefully controlling the preparation conditions, we find chemical preparation methods (i.e., DPU and DPN) can achieve uniform growth of monodispersed Au nanoparticles on MnO_2 nanowires (Au/MnO_2) same as sputtering; moreover, the as-prepared Au–MnO_2 by DPU and DPN shows stronger interaction than that by sputtering, thereby achieving higher OER performance. Delicate chemical valence change and conductivity improvement induced by such interaction are further quantified by conventional XPS, resistivity and impedance measurements.

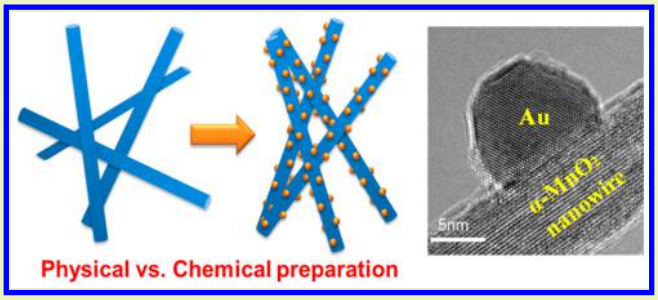

KEYWORDS: *Oxygen evolution reaction (OER), Water electrolysis, Manganese oxide nanowire, Au nanoparticles, Trivalent manganese*

INTRODUCTION

Splitting water into hydrogen and oxygen via electrocatalytic or photocatalytic routes has been considered as a feasible way to store renewable energy (e.g., wind and solar energies) into the form of energy-intense chemical fuels.[1−3] One of the prerequisites of global scale employment of water splitting devices is to develop a robust, durable and highly efficient electrocatalyst. As the half reaction of water splitting, electrochemical water oxidation, also known as the oxygen evolution reaction (OER), is currently considered a major bottleneck. Substantial overpotentials typically in excess of 450 mV are required to drive the sluggish four-electron OER process. According to the well-known "volcano plot" of electrocatalysts, precious metal oxides including PtO_2, IrO_2 and RuO_2 possess the highest electrocatalytic activity among various metals.[4,5] Nevertheless, their prohibitive price and scarcity limit widespread implementation of these materials. On the other hand, earth abundant metal oxides mainly the first-row transitional metal have been extensively studied. One typical example is MnO_2, which has already shown a decent electrochemical activity.[6−10] It also possesses low toxicity whereas Ni and Co are potentially carcinogenic.[11,12] Moreover, the basic MnO_6 octahedron unit can build up a rigid MnO_2 framework with unique one-, two-, or three-dimensional (1D, 2D or 3D) tunnels, generating a large diversity in the crystalline structure MnO_2 and thereby tunable physicochemical properties.[13] All those advantages make MnO_2 as a highly promising OER candidate with strong designability and scalability.[14,15]

Dispersion of fine Au nanoparticles (AuNPs) on certain metal oxide support has been reported exhibiting surprisingly high catalytic activity toward various chemical reactions (e.g., alcohol oxidation).[16−19] So far, anchoring AuNPs onto metal oxide substrates such as NiO_x, $NiCo_2O_4$ and MnO_x, have been demonstrated promoting the OER performance only in several

Received: April 18, 2015
Revised: July 13, 2015
Published: August 3, 2015

DOI: 10.1021/acssuschemeng.5b00324
ACS Sustainable Chem. Eng. 2015, 3, 2049−2057

recent literatures.[20,21] T. F. Jaramillo et al. reported that deposition of fine Au nanoparticles on MnO_x thin films via physical sputtering method can remarkably promote the OER activity with comparison to MnO_x in the absence of Au, generating 1 order of magnitude higher turnover frequency (TOF) than that of pure MnO_x.[21] On the basis of the *in situ* and *ex situ* spectroscopic XAS (X-ray absorption spectroscopy), Jaramillo et al. concluded that such significant enhancement is due to the strong localized interfacial interactions between Au and MnO_x. MnO_x located away from the interface with Au owns a more reduced state than MnO_x located near Au, which probably benefits the OER. R. Frydendal et al. also proposed a theoretical explanation for these enhancements based on a hydrogen acceptor concept, which comprises a stabilization of an *−OOH intermediate by Au, effectively lowering the potential needed for breaking bonds to the surface.[22] However, there are still many issues remaining. From the viewpoint of scientific understanding, AuNPs with high electron negativity may strongly change the physiochemical properties of MnO_2 nanostructures with their high surface-to-volume ratio, which have been discovered in several semiconductor nanostructures.[20,23] These physiochemical changes such as chemical valence and conductivity variation need to be further quantified rather than qualified in order to reveal the in-depth structure-performance relationship. Moreover, from technological points of view, it is also attractive to explore more cost-effective routes to deposit AuNPs such as wet chemical methods to replace physical sputtering in order to facilitate possible future commercialization of electrocatalysts. Wet chemical methods may also generate different levels of interaction between Au and MnO_2 in comparison with physical methods, since Au precursors and deposition mechanism are totally different.

In this report, we addressed aforementioned scientific and technological issues by deposition of AuNPs on MnO_2 nanowires (Au/MnO_2) with high surface-to-volume ratio via different chemical and physical methods, including physical sputtering (PS), deposition-precipitation with urea (DPU), DP with NaOH (DPN) and deposition-reduction (DR) with $NaBH_4$. We find that chemical methods (i.e., DPU and DPN) can achieve growth of monodispersed AuNPs on MnO_2 nanowires same as physical sputtering; furthermore, in comparison with sputtering, DPN and DPU methods result in stronger interaction between Au and MnO_2, thereby demonstrating better OER performances. The enhanced interactions indeed lead to pronounced physicochemical changes of MnO_2 nanowires. Such changes mainly including Mn valence change and conductivity improvement have been successfully quantified via XPS, resistivity and impedance measurements.

EXPERIMENTAL SECTION

Materials. Chemical reagents of analytical grade including $MnSO_4 \cdot H_2O$, $(NH_4)_2S_2O_8$, $(NH_4)_2SO_4$, $NaBH_4$, $HAuCl_4$, urea and polyvinylpyrrolidone (PVP, molecular weight 25 000−30 000) were purchased from Sinopharm Chemical Reagent Co., Ltd. and used as-received.

Preparation of α-MnO_2 Nanowires. α-MnO_2 nanowires were synthesized by a typical hydrothermal method according to the reported procedure.[24,25] 0.02 mol of $MnSO_4 \cdot H_2O$, 0.02 mol of $(NH_4)_2S_2O_8$ and 0.08 mol of $(NH_4)_2SO_4$ were added to 70 mL of deionized water with vigorous stirring to form a clear transparent precursor solution. The mixed solution was transferred to a 100 mL Telfon-lined stainless autoclave, and then heated at 140 °C for 12 h. After being cooled to room temperature, the obtained precipitate was filtered and washed with a large amount of water until the pH value of wastewater reached around 7. MnO_2 nanowire powder was obtained after drying the precipitate in the oven at 120 °C for 16 h. To demonstrate the α-MnO_2 owning the best OER activity, nanostructured MnO_2 with other crystalline structures including β-, γ- and δ- MnO_2 were also synthesized for comparison (preparation details seen in the Supporting Information).

Preparation of Au/MnO_2 Catalysts. Gold was deposited on α-MnO_2 nanowires (denoted as Au/MnO_2) by various methods as described below.

a. Physical Sputtering (PS). Deposition of AuNPs via PS is a matured technique.[26,27] α-MnO_2 nanowires were first coated on the carbon paper (CP) via dip coating. Afterward, gold was deposited by a DC planar magnetron sputtering system with the sputtering time of 45 s, discharge power of 50 W, total Ar pressure of about 0.3 Pa and the electrode distance of 50 mm. The sample was denoted as PS-Au/MnO_2.

b. Deposition−Precipitation with Urea (DPU). In a typical preparation,[28,29] 1 g of α-MnO_2 nanowires was dispersed in 100 mL of aqueous mixed solution of $HAuCl_4$ (7.5 mM) and urea (0.75M). The mixed solution was kept at 80 °C with vigorously stirred for 4 h. Then, the products were collected by centrifugation and washed with deionized water. Afterward the products were vacuum-dried at 60 °C for 12 h and calcinated at 300 °C for 2 h. The sample was denoted as DPU-Au/MnO_2-C (C means calcination).

c. Deposition−Precipitation with NaOH (DPN). At first, 100 mL of 7.5 mM $HAuCl_4$ aqueous solution was adjusted to 8 with addition of 1 M NaOH. Then, 1 g of α-MnO_2 nanowires was added to the solution and the pH of the solution was kept constant around 8 by dropwise addition of 1 M NaOH. Meanwhile, the aqueous solution was heated to 80 °C with vigorous stirring for 2 h. Afterward, the products were collected by centrifugation, washed and dried same as the DPU sample. The sample was named as DPN-Au/MnO_2.

d. Deposition−Reduction by $NaBH_4$ Protected by PVP (DR). The DR-Au/MnO_2 sample was prepared by using $NaBH_4$ as the reducing agent.[30] 60 mg PVP were added to 10 mL of 7.5 mM $HAuCl_4$ aqueous solution and then stirred for 30 min at room temperature. After that, 200 mg of MnO_2 was dispersed into the solution and stirred for another 30 min. Then, an aqueous solution of $NaBH_4$ (10 mL including 59.8 mg $NaBH_4$) was added at a rate of one drop in every three seconds under vigorous stirring for about 10 min. The solutions were stirred for another 1 h. Finally, the products were collected, washed and dried same as the DPU sample.

Characterizations. The phase purity of the Au/MnO_2 catalysts was identified by powder X-ray diffraction (XRD) using Cu Kα radiation (λ= 0.154 178 nm) with a scanning speed of 4°/min. The N_2 adsorption−desorption isotherm was measured on a Micrometrics system. Surface areas of the Au/MnO_2 catalysts were determined by the Brunauer−Emmett−Teller (BET) gas adsorption method. The size and morphology of the Au/MnO_2 catalysts were observed using a FEI Tecnai G2 transmission electron microscopy (TEM). Element dispersion and Au loading were investigated by Scanning electron microscope (SEM, Hitachi S-520) and energy dispersive spectrum (EDS). The X-ray photoelectron spectra (XPS) were recorded on a Thermo Scientific K-Alpha XPS spectrometer using Al Kα X-ray source. Calibration of binding energy was carried out by setting binding energy of C 1s peak to 284.8 eV. Electrical conductivity of MnO_2 nanowires and as-prepared Au/MnO_2 catalysts were measured by a standard four-point probe.

Electrochemical Measurements. 5 mg of Au/MnO_2 catalyst power was dispersed in 1 mL of 3:1 v/v water/isopropyl alcohol solution mixed solvent with 16 μL of 5 wt % Nafion solution (5 wt %, Sigma-Aldrich). Then, the mixture was ultrasonicated for about 30 min to generate a homogeneous ink. After that, 20 μL of the ink was transferred onto the carbon paper (CP). The catalyst loading area was strictly controlled ~1 cm^2. Finally, the as-prepared catalyst film was baked at 60 °C for 30 min and used as the working electrode. Electrochemical measurements were performed on a potentiostat (PARSTAT 4000, Ametek) at room temperature in a three electrode configuration using a Pt plate and an Ag/AgCl (3 M KCl) electrode as

DOI: 10.1021/acssuschemeng.5b00324
ACS Sustainable Chem. Eng. 2015, 3, 2049−2057

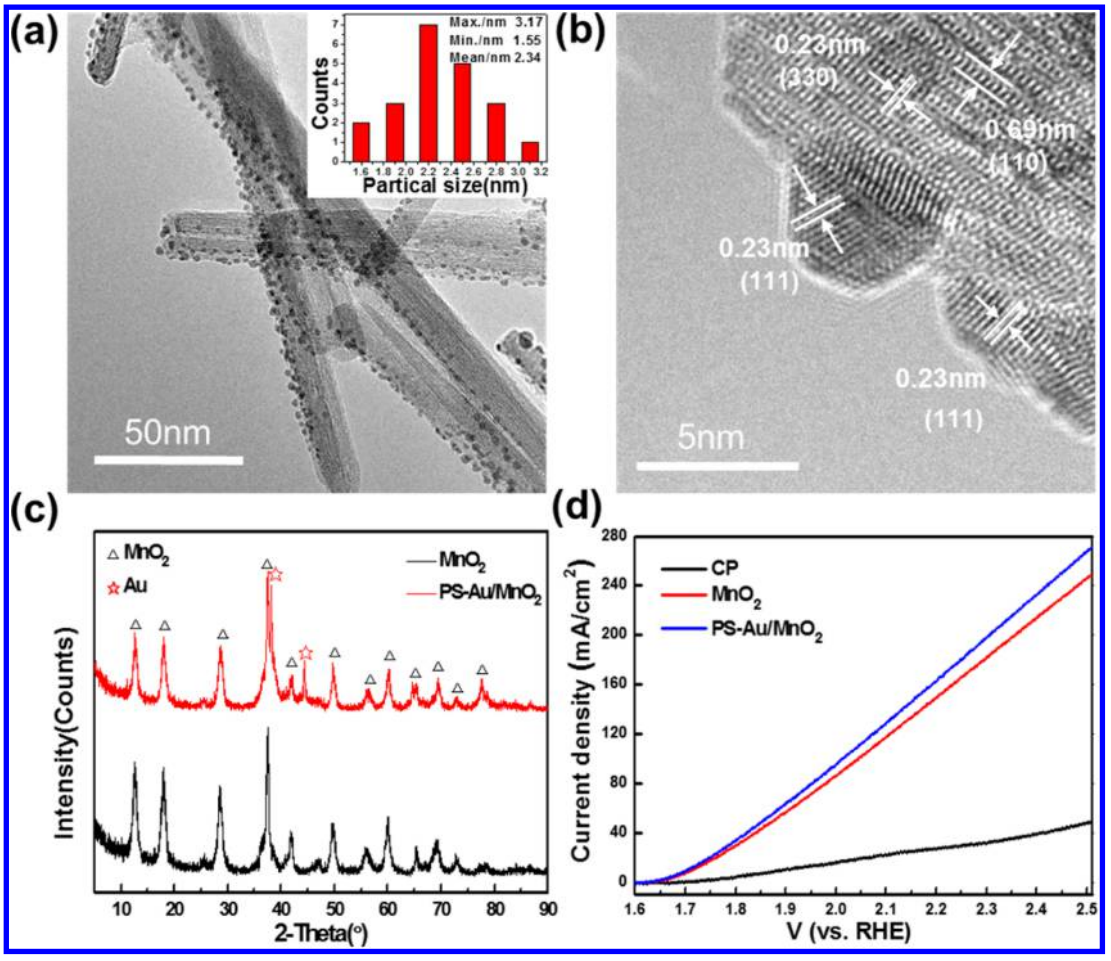

Figure 1. (a) TEM image of PS-Au/MnO_2 catalyst and the size distributions of Au nanoparticles (inset) obtained for PS-Au/MnO_2; (b) HRTEM image of PS-Au/MnO_2 catalyst; (c) XRD patterns of MnO_2 and PS-Au/MnO_2; (d) LSVs of carbon paper (CP), as-prepared MnO_2 and PS-Au/MnO_2.

the counter and reference electrodes, respectively. Linear scan voltammograms (LSV) were measured with a scanning rate of 50 mV/s. The quasi-stationary polarization curves for Tafel measurements were recorded with a scanning rate of 0.33 mV s^{-1} and the slope of the capacitive current was determined by the Versa Studio software. All potential values were calibrated to the reversible hydrogen electrode (RHE) according to the equation E(V vs RHE) = E(V vs Ag/AgCl)+1.01 V (details seen in Figure S1). The electrochemical impedance spectroscopy (EIS) test were carried out in N_2-saturated 1 M KOH solution under an anodic polarization potential of 0.6 V (vs Ag/AgCl). The EIS spectrum was obtained in a frequency range of 0.1−10^5 Hz with an amplitude of 5 mV. The charge transfer resistance (R_{ct}) was determined by fitting the Nyquist plot to a Randles' equivalent circuit.

RESULTS

Because MnO_2 has diverse crystalline structures, we first synthesized and compared four typical phases, including α-, β-, γ- and δ-MnO_2 (see in Figure S2 and Figure S3). The α-MnO_2 nanowire prepared via conventional hydrothermal method possesses the highest OER activity among four phases, in line with recent literature reports.[15,24,25] Figure S2 shows the TEM images and XRD pattern of α-MnO_2 nanowires. The averaged diameter of the α-MnO_2 nanowires was about 9.0 nm and the measured BET surface area was 94.3 m^2/g. Taking its relatively high electrochemical activity and surface-to-volume ratio into consideration, we chose the α-MnO_2 nanowire for further investigating the interactions between Au and MnO_2.

PS-Au/MnO_2. Sputtering is a physical process whereby Au atoms are ejected from a solid target due to bombardment of the target, and impact energetically on the substrate resulting in the formation of Au nanoparticles or films.[31] Figure 1a shows the TEM image of PS-Au/MnO_2. Extremely fine AuNPs were highly dispersed on the one side (facing the Au target) of α-MnO_2 nanowires, and the size distribution ranges from 1.55 to 3.17 nm for PS-Au/MnO_2, as depicted in inset of Figure 1a. Accordingly, the mean gold particle sizes are estimated to be 2.34 nm for Au/MnO_2 and the Au loading is about 12 wt % confirmed by SEM-EDS. High-resolution TEM (HRTEM) was employed to study the interface between AuNPs and α-MnO_2 nanowires seen in Figure 1b. The HRTEM images clearly show the lattice fringes of AuNPs and α-MnO_2 nanowires, indicating their nice crystallinity. The interlayer spacing of 0.23 nm agreed with (330) planes of MnO_2 and (111) planes of Au.[32] We also observed that there are lattice mismatches between Au and MnO_2. The XRD patterns shown in Figure 1c verify the TEM results: the crystalline structure of α-MnO_2 wires remained unchanged after sputtering, the metallic Au diffraction peaks were clearly evidenced.

Figure 1d shows the OER performances of conductive CP substrate, and α-MnO_2 nanowires before and after sputtering, measured by the LSV in 1 M KOH solution. The CP demonstrates weak OER activity. The current density of α-

DOI: 10.1021/acssuschemeng.5b00324
ACS Sustainable Chem. Eng. 2015, 3, 2049−2057

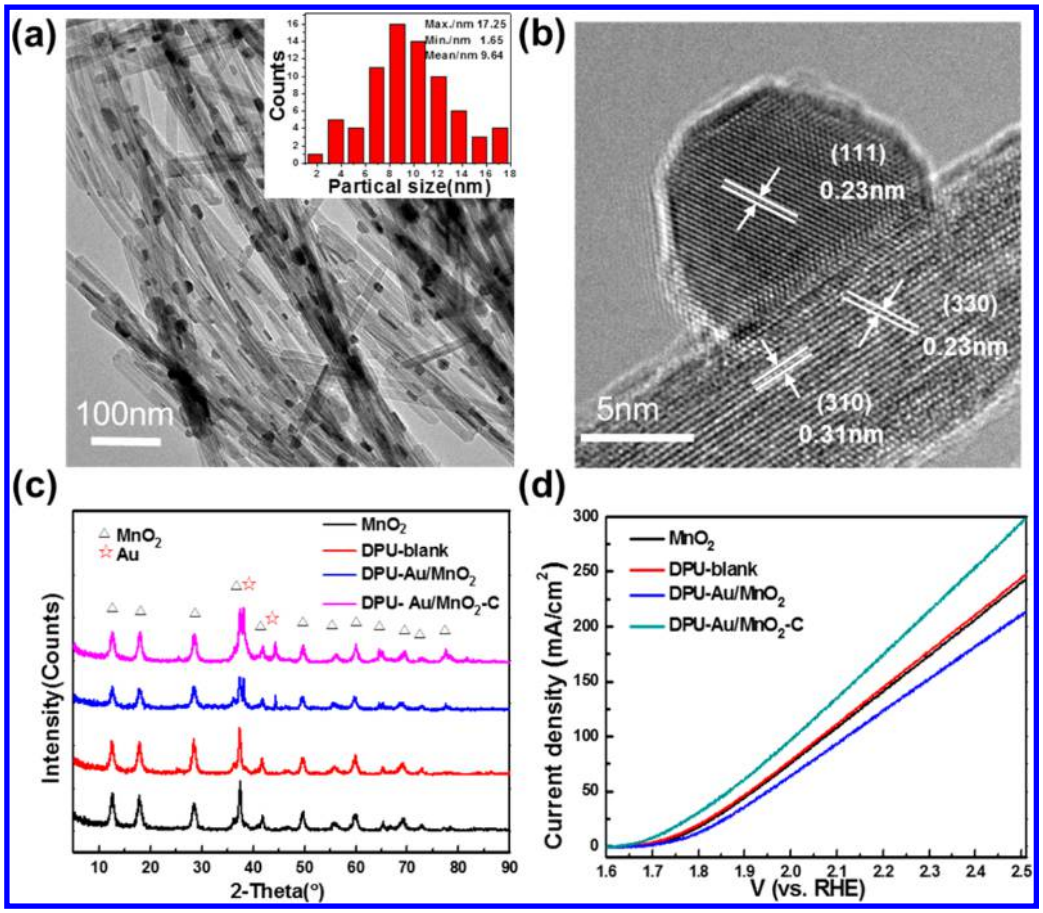

Figure 2. (a) TEM image of DPU-Au/MnO_2-C catalyst and the size distributions of Au nanoparticles (inset) obtained for DPU-Au/MnO_2-C; (b) HRTEM image of DPU-Au/MnO_2-C catalyst; (c) XRD patterns of DPU-Au/MnO_2, DPU-blank, DPU-Au/MnO_2 and DPU-Au/MnO_2-C; (d) LSVs of MnO_2, DPU-blank, DPU-Au/MnO_2 and DPU-Au/MnO_2-C.

MnO_2 nanowires at 2.51 V (vs RHE) increased by 34.5 mA/cm^2 after Au sputtering.

DPU-Au/MnO_2. Au/MnO_2 catalyst was prepared by DPU by slightly optimizing the recipe reported in in literature.[28] Reactions of the DPU method is as follows:

$$CO(NH_2)_2 + 3H_2O \rightarrow CO_2 + 2NH_4^+ + 2OH^- \quad (1\text{-}1)$$

$$AuCl_4^- + nOH^- \rightarrow [Au(OH)_nCl_{4-n}]^- + nCl^- \ (n = 1{-}3) \quad (1\text{-}2)$$

$$[Au(OH)_nCl_{4-n}]^- + (3-n)OH^- \rightarrow Au(OH)_3 + (4-n)Cl^- \ (n = 1{-}3) \quad (1\text{-}3)$$

The pH value of the starting gold chloride solution is around 2. When the pH of the solution was raised to a value between 6 and 10, the partially hydrolyzed species $[Au(OH)_nCl_{4-n}]^-$ (n = 1−3), then nucleate at the surface of MnO_2 to form $Au(OH)_3$. AuNPs were eventually formed after calcination. The pH change of the solution during DPU is shown in Figure S4. The TEM images of Au/MnO_2 formed by DPU and subsequent calcination (DPU-Au/MnO_2-C) are shown in Figure 2a,b. Similar with sputtering, DPU method is also capable of anchoring fine AuNPs uniformly on the α-MnO_2 nanowires. The size distribution ranges from 1.65 to 17.25 nm as shown in inset of Figure 2a, and the mean size of AuNPs formed by DPU is estimated to be 9.64 nm, much bigger than that by sputtering. The Au loading was around 11 wt % measured by SEM-EDS. Moreover, as shown in the HRTEM image in Figure 2b, we observed continuous lattice fringes extended from α-MnO_2 to AuNPs, corresponding to the (330) and (111) lattice planes of MnO_2 and AuNPs with same d-spacing of 0.23 nm, which are different from lattice mismatches observed at the interface between Au and MnO_2 in the PS sample. It suggests potential epitaxial growth of AuNPs on α-MnO_2, and such atomic binding will probably benefit the OER activity of the Au/MnO_2 composite. The XRD patterns (see in Figure 2c) confirm that the presence of metallic Au and the crystalline structure of α-MnO_2 wires remained unchanged after chemical deposition.

Figure 2d shows the LSV of the as-prepared pure MnO_2, DPU-blank (without Au deposition), DPU-Au/MnO_2 (without calcination) and DPU-Au/MnO_2-C samples. The OER performance of DPU-black sample is same as that of original α-MnO_2 wires, indicating the solution process does not affect the intrinsic electrochemical properties of α-MnO_2 wires. Interestingly, there is a degradation of the OER performance for DPU-Au/MnO_2, because Au is in the form of $Au(OH)_3$. This phenomenon indicates the metallic state of Au is crucial for improving the OER activity of MnO_2. After calcination, we find that the enhancement of the OER performance is significant. The current density of DPU-Au/MnO_2-C increased by more than 60.0 mA/cm^2. In contrast, further calcination on the PS-Au/MnO_2 leads to degradation of the OER performance (see Figure S5), suggesting that heat treatment in the air would not benefit the Au/MnO_2 samples with Au already existing as the metallic phase.

DOI: 10.1021/acssuschemeng.5b00324
ACS Sustainable Chem. Eng. 2015, 3, 2049−2057

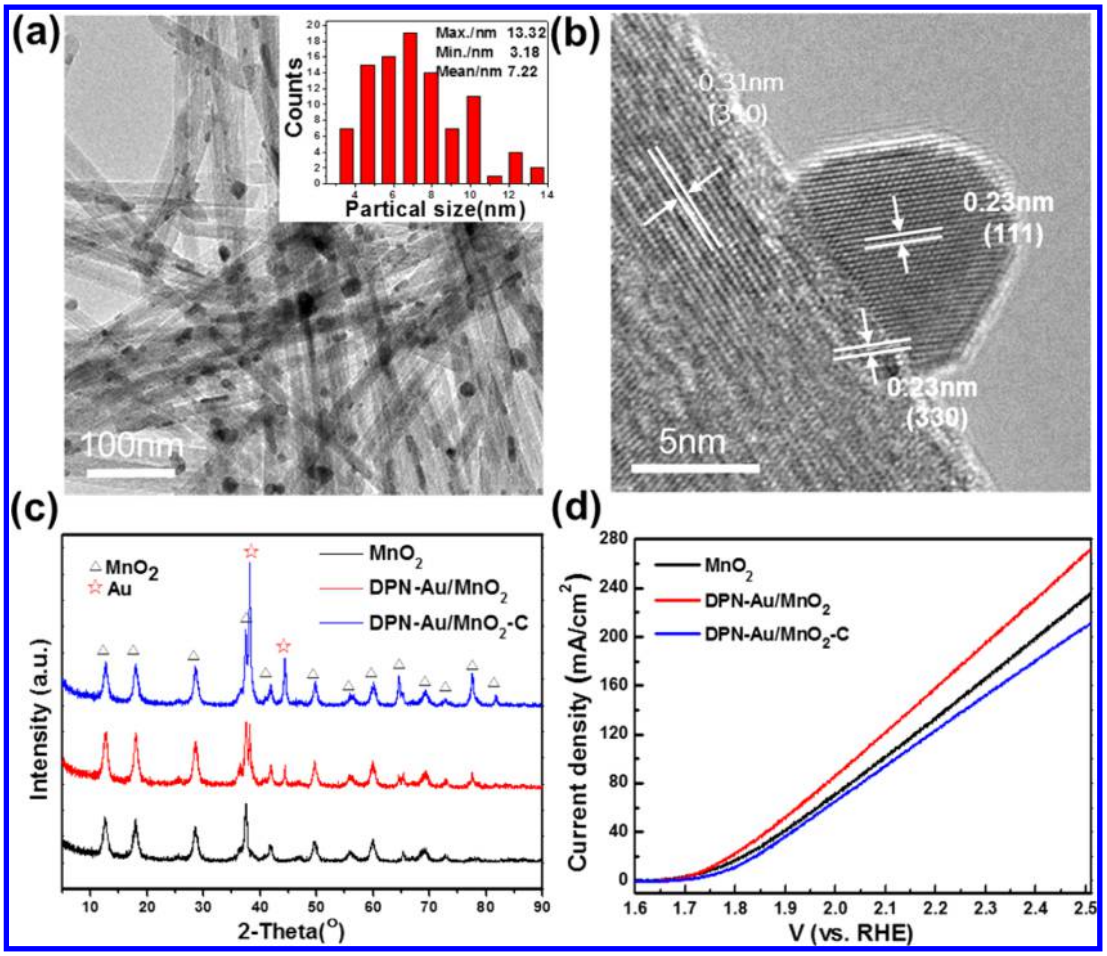

Figure 3. (a) TEM image of DPN-Au/MnO_2 catalyst and the size distributions of Au nanoparticles (inset) obtained for DPN-Au/MnO_2; (b) HRTEM image of DPN-Au/MnO_2 catalyst; (c) representative powder of XRD patterns of various catalysts; (d) LSVs of MnO_2, DPN-Au/MnO_2 and DPN-Au/MnO_2-C.

DPN-Au/MnO_2. DPN method uses NaOH instead of urea as the precipitant.[29] The pH value of the solution is relatively high and keeps almost constant around 8 during reaction. The high pH value leads to fast precipitation of $Au(OH)_3$, and the formed $Au(OH)_3$ afterward is thermally decomposed to Au within the same reaction time. Reactions of the DPU method is as follows:

$$AuCl_4^- + 3OH^- \rightarrow Au(OH)_3 + 4Cl^- \quad (2\text{-}1)$$

$$Au(OH)_3 \rightarrow Au + 3OH^- \quad (2\text{-}2)$$

Highly monodispersed AuNPs with mean AuNP size of 7.22 nm are loaded on α-MnO_2 wires (see Figure 3a,b). Similar as the DPU sample, the crystal lattice well extended from AuNPs to MnO_2 nanowires, suggesting the potential epitaxial growth of AuNPs on MnO_2. The metallic phase of Au was also confirmed via XRD (see Figure 3c).[33] The Au loading was 9 wt % measured by SEM-EDS. Figure 3d shows the OER performance of DPN-Au/MnO_2. The current density of DPN-Au/MnO_2 at 2.51 V (vs RHE) reached 272.3 mA/cm^2, which is ~30 mA/cm^2 higher than that for the original MnO_2 nanowires.

DR-Au/MnO_2. DR with PVP as surfactant is a commonly used method to prepare Au nanoparticles and colloids.[26] The reaction is as follows:

$$2AuCl_4^- + 2BH_4^- + 4H_2O \rightarrow 2Au + 2BO_2^- + 8Cl^- + 6H^+ + 5H_2\uparrow \quad (3\text{-}1)$$

Figure 4a,b shows the TEM images of the obtained DR-Au/MnO_2 under the optimal condition as previous literatures reported. AuNPs are weakly attached to the α-MnO_2 wires and there is no evidence of close binding between both AuNPs and nanowires. The mean gold particle sizes are estimated to be 14.33 nm, much larger than all above-mentioned samples. Moreover, Au loading is only 3 wt % as confirmed by SEM-EDS. The XRD patterns shown in Figure 4c reveals the metallic phase of Au. The existence of the protecting surfactant PVP on the surface of AuNPs is possibly the major reason for the weak binding and low Au loading. Figure 4d shows the OER performance. In comparison with the original α-MnO_2 wires, the current density of DPN-Au/MnO_2 at 2.51 V (vs RHE) only increased by ~10 mA/cm^2.

DISCUSSION

All above results clearly suggest that Au can greatly promote the OER activity of MnO_2, and the preparation methods indeed have major impacts on the final performance. Table 1 lists the surface area, current density (at 2.51 V (vs RHE)), TOF (calculated based on the surface area and current density, details seen in Supporting Information), and Au loading of all samples. The current density, TOF value and Tafel slope clearly

DOI: 10.1021/acssuschemeng.5b00324
ACS Sustainable Chem. Eng. 2015, 3, 2049−2057

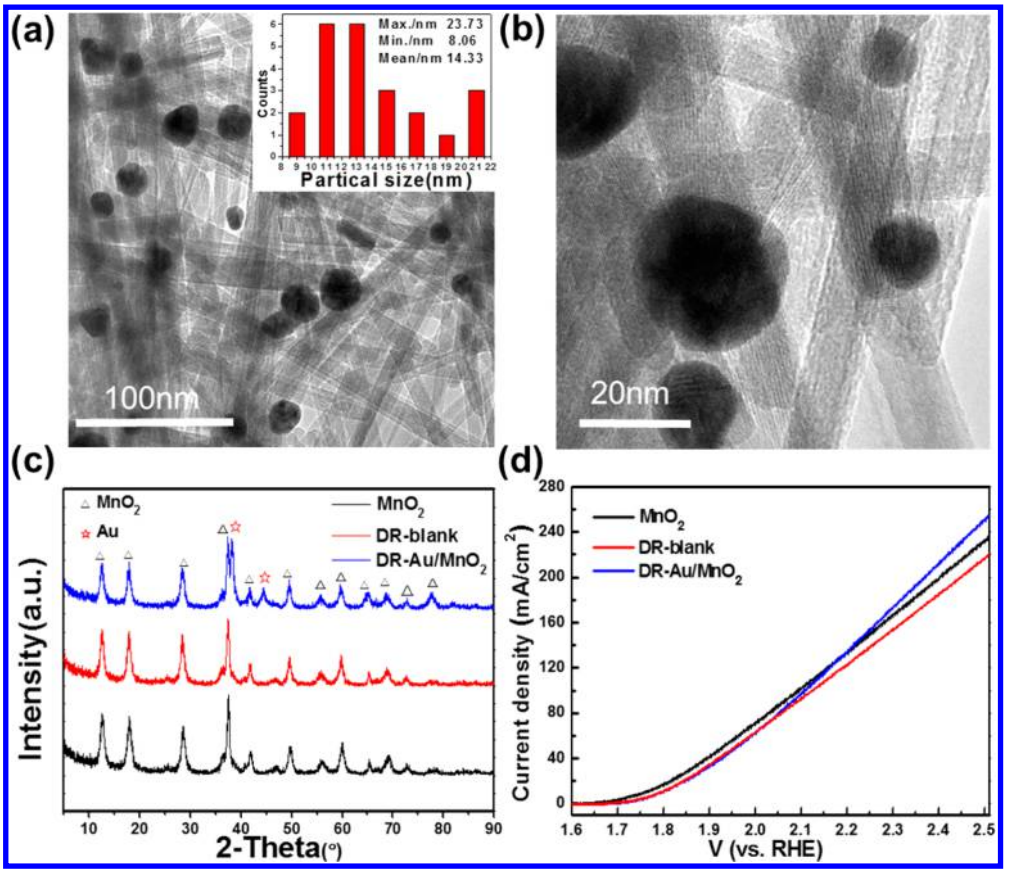

Figure 4. (a) TEM image of DR-Au/MnO_2 catalyst and the size distributions of Au nanoparticles (inset) obtained for DR-Au/MnO_2; (b) TRTEM image of DR-Au/MnO_2 catalyst; (c) XRD patterns of MnO_2, DR-blank and DR-Au/MnO_2; (d) LSVs of MnO_2, DR-blank and DR-Au/MnO_2.

Table 1. Comparison of Different Parameters of Five Samples Including Original MnO_2, PS-MnO_2, DPU-Au/MnO_2-C, DPN-Au/MnO_2 and DR-Au/MnO_2

sample name	surface area(m^2/g)	Au loading[a] (wt %)	resistivity[b] (Ω)	R_{ct}[b] (Ω)	current[c] (mA/cm^2)	TOF[d] (s^{-1})	Tafel slope (mV/decade)
MnO_2	94.3	0	2E5	360.1	236.3	0.53	72
PS-Au/MnO_2	N/A	12	N/A	141.8	270.8	0.61	62
DPU-Au/MnO_2-C	68.1	11	280	23.6	299.5	0.67	51
DPN-Au/MnO_2	79.1	9	300	65.2	272.3	0.61	57
DR-Au/MnO_2	66.4	3	5E3	191.8	254.3	0.57	68

[a]The theoretical Au loading was 12.5 wt % and the actual Au loading was confirmed by SEM-EDS. [b]Resistivity is the resistance of the Au/MnO_2 catalyst and measured by four point probe. R_{ct} is the charge transfer resistance and obtained by fitting the EIS data. [c]The current density was measured at 2.51 V (vs RHE). [d]The turnover frequency (TOF) was calculated by the model as described in the Supporting Information.

confirm that the intrinsic electrochemical activity of different samples follows the order of DPU-Au/MnO_2-C > DPN-Au/MnO_2 ≈ PS-Au/MnO_2 > DR-Au/MnO_2 > MnO_2 (see in Figure S6a–c).[33] It is worth noting that the mean size of AuNPs for DPU-Au/MnO_2-C and DPN-Au/MnO_2 is even bigger than those for PS-Au/MnO_2, whereas the Au loadings for these three samples are comparable. This phenomenon implies that the AuNPs size is not a key factor influencing the OER. Therefore, we considered that different levels of interactions between Au and MnO_2 play a major role in determining the final OER performance.

In support of this interpretation, we first conducted resistivity measurements (see in Figure S6d), because the intrinsic conductivity of nanomaterials is a critical parameter influencing the OER performance. As listed in Table 1, MnO_2 nanowires undergoes two magnitudes reduction of resistivity after AuNP deposition. The resistivity also varies depending on preparation methods. Because MnO_2 is a semiconductor material, Schottky junctions are formed after anchoring AuNPs.[34,35] Because of equilibration of the Fermi levels of AuNPs and α-MnO_2, charge carriers would transfer from metal NPs to semiconducting MnO_2, resulting in the conductivity improvement of MnO_2. Such phenomenon has been discovered and verified in several semiconducting nanomaterials such as Si and VO_2, commonly named as "surface doping effect".[36,37] This effect is negligible for bulk semiconducting materials, however it is significant for nanomaterials owing to their high surface-to-volume ratio. Here, the resistivity of DPU-Au/MnO_2-C is slightly lower than that of DPN-Au/MnO_2, and 17.8 times lower than that of DR-Au/MnO_2. We ascribed the enhanced conductivity to the higher quality binding in the atomic scale and stronger interactions between Au and MnO_2 nanowires in DPU-Au/MnO_2-C in comparison with other samples. Stronger interaction would provide more charge carriers to MnO_2

DOI: 10.1021/acssuschemeng.5b00324
ACS Sustainable Chem. Eng. 2015, 3, 2049–2057

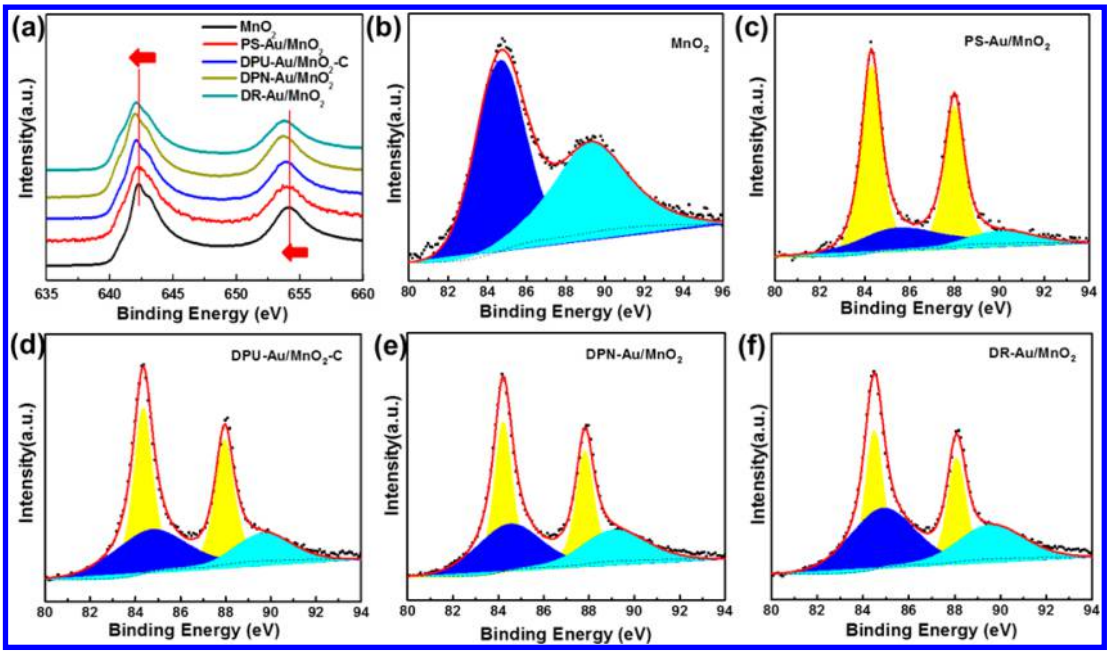

Figure 5. XPS spectra of Au 4f and Mn 3s for different Au/MnO_2. (a) Mn 2p of Au/MnO_2. (b) DPU-Au/MnO_2-C, (c) DPN-Au/MnO_2, (d) DR-Au/MnO_2. The yellow area indicated the Au $4f_{7/2}$ (high) and Au $4f_{5/2}$ (low) spectra, the sky blue area indicates the Mn 3s spectra.

Table 2. XPS Peak Analyses of Au/MnO_2 Catalysts Prepared by Various Methods

	Au 4f (eV)		Mn 3s (eV)			
sample	$4f_{7/2}$	$4f_{5/2}$	$3s_{3/2}$	$3s_{1/2}$	ΔE	average valence[a]
MnO_2			84.65	89.20	4.55	3.92
PS-Au/MnO_2	84.29	87.99	85.54	90.18	4.64	3.81
DPU-Au/MnO_2-C	84.35	87.95	84.60	89.71	5.11	3.26
DPN-Au/MnO_2	84.22	87.82	84.43	89.11	4.68	3.76
DR-Au/MnO_2	84.48	88.08	84.81	89.61	4.80	3.62

[a]The average valence of Mn was calculated by the equation described below:

$$\Delta E \approx 7.88 - 0.85n$$

where ΔE is the Mn 3s multiplet splitting energies and n ($2 \leq n \leq 4$) is the average oxidation state of the Mn atoms.[43]

nanowires leading to conductivity enhancement. EIS tests offer more insight of the resistivity influence on the reaction kinetics.[38] Through fitting the Nyquist plot into a Randles' equivalent circuit (see Figure S7), the R_{ct} values were obtained (listed in Table 1) and follow the order: DPU-Au/MnO_2-C < DPN-Au/MnO_2 < PS-Au/MnO_2 < DR-Au/MnO_2 < MnO_2. Such order well matches the trend of the measured sample resistivity, clearly illustrating that the electron transfer process during the OER is strongly influenced by the sample conductivity.

To support further our interpretation, X-ray photoelectron spectroscopy (XPS) measurements were carried out to examine delicate surface chemistry changes of MnO_2 after depositing AuNPs via different methods, because different levels of interactions would also lead to varying degrees of chemical valence change. The Mn $2p_{3/2}$ peaks of all samples all exhibit highly asymmetry (see Figure 5a), suggesting the presence of multiple Mn oxidation state.[33] We also observed that the Mn 2p peak of DPU and DPN samples with enhanced interaction shifted to the lower energetic binding energies (BEs), indicating the decrease of Mn valence.[39] However, it is hard to accurately determine the oxidation state of Mn purely by the Mn 2p peak, because the splitting between Mn^{3+} and Mn^{4+} is less than 1 eV.[40] The extent of Mn 3s doublet splitting can give more precise information than Mn 2p does. Unfortunately, the Au 4f doublet overlaps with the Mn 3s multiplet splitting peaks from the support.[32] Through assuming the same Mn 3s/Mn 2p intensity ratio for all Au attached samples and constraining the relative position and intensity of the two Au $4f_{7/2}$ and Au $4f_{5/2}$ components to the respective expected BE of 3.6 eV and 1.33, the peak position and area of the Au 4f and Mn 3s doublet can be successfully obtained via curve fitting procedure (see Figure 5b–d).[41] According to the previous literature,[19] the BE separation between the two peaks of the Mn 3s doublet (ΔE 3s) shows an inverse linear relationship with the averaged Mn valence (υ_{Mn}).

Table 2 lists the calculated υ_{Mn} values of all samples, and indeed υ_{Mn} shows strong dependence on the preparation method.[42] According to recent reports, Mn^{3+} in the MnO_2 can greatly promote the OER activity, because the electronic configuration of Mn^{3+} in the MnO_2 provides $t_{2g}^3e_g^1$ configuration, leading to the degenerated e_g orbitals asymmetrically filled in the high-spin state.[44,45] The high spin state with e_g^1 in the Mn can be oriented toward the OH^- group thereby improving the OER activity. The fraction of Mn^{3+} in all samples follow the order: DPU-Au/MnO_2-C > DR-Au/MnO_2

DOI: 10.1021/acssuschemeng.5b00324
ACS Sustainable Chem. Eng. 2015, 3, 2049–2057

> DPN-Au/MnO_2 > PS-Au/MnO_2 > MnO_2. This order mainly agrees with the order of the OER activity with the exceptional case of DR-Au/MnO_2, because of the very weak binding between Au and MnO_2 in the DR sample. Nevertheless, such results provide the evidence that the interaction between Au and MnO_2 strongly depends on the preparation methods. Enhanced interactions leads to the better conductivity and increased fraction of Mn^{3+}, thereby greatly promoting the corresponding electrochemical activity of Au/MnO_2.

Because the DPU method is proven as the best among physical and other chemical methods, we tried to understand the uniqueness of this method. We measured the pH value change during precipitation. The pH of the DPU solution grew slowly from 2 to 7 because the release of OH^- for urea is a relatively slow process, while the pH value of DPN was almost keeping constant around 8. The slow growth of AuNPs may benefit the atomic binding between Au and MnO_2, resulting in stronger interaction than other chemical and physical methods.

CONCLUSION

In this report, we have successfully anchored AuNPs on α-MnO_2 nanowires via different physical and chemical methods, including PS, DPU, DPN and DR. DPU and DPN methods can not only deposit monodispered AuNPs on MnO_2 but also achieve higher quality binding between Au and MnO_2 in the atomic scale than the PS method. Through systematical comparing of the OER performance, we found that the preparation methods exert strong influence on the interaction between Au and MnO_2. The extent of such interaction directly determines two crucial factors for the OER including conductivity and chemical valence of Mn (fraction of Mn^{3+}). The interaction strength and the OER activity follow the order: DPU-Au/MnO_2-C > DPN-Au/MnO_2 ≈ PS-Au/MnO_2 > DR-Au/MnO_2. Our approaches not only provide in-depth scientific understanding of Au/MnO_2 composite electrocatalysts through quantifying the physiochemical changes of MnO_2 caused by the unique interaction between Au and MnO_2 but also pave the technological way of preparing better Au/MnO_2 electrocatalysts in a cost-effective wet chemical way rather than complex physical methods.

ASSOCIATED CONTENT

Supporting Information

The Supporting Information is available free of charge on the ACS Publications website at DOI: 10.1021/acssuschemeng.5b00324.

Calculation details of turnover frequency, RHE calibration, detailed preparation of β-, γ-, δ-MnO_2, cyclic voltammetry for the RHE calibration (Figure S1), TEM images of β-, γ-, δ-MnO_2 (Figure S2), TEM images and XRD pattern of α-MnO_2 nanowires (Figure S3), pH change during DPU (Figure S4), LSV curve of PS-Au/MnO_2 (Figure S5), OER activity evaluation of different samples (Figure S6), Nyquist plot (Figure S7), and XPS peak position of Mn 2p (Table S1) (PDF).

AUTHOR INFORMATION

Corresponding Authors

*X. Li. E-mail: lixp@sari.ac.cn.

*T. Zhao. E-mail: zhaotj@sari.ac.cn.

Notes

The authors declare no competing financial interest.

ACKNOWLEDGMENTS

This work was supported by SARI Interdisciplinary Research funding (No. Y426475231), National Natural Science Foundation of China (NSFC No. 21403280). Y. Zhao is grateful for the financial support from the NSFC No. 21403277 and Shanghai Natural Science Foundation (No. 14ZR1444600). T. Zhao acknowledges the support from CAS hundred talent program.

REFERENCES

(1) Carmo, M.; Fritz, D. L.; Mergel, J.; Stolten, D. A comprehensive review on PEM water electrolysis. *Int. J. Hydrogen Energy* **2013**, *38*, 4901−4934.

(2) Li, X.; Xiao, Y.; Bang, J. H.; Lausch, D.; Meyer, S.; Miclea, P. T.; Jung, J. Y.; Schweizer, S. L.; Lee, J. H.; Wehrspohn, R. B. Upgraded silicon nanowires by metal-assisted etching of metallurgical silicon: a new route to nanostructured solar-grade silicon. *Adv. Mater.* **2013**, *25*, 3187−3191.

(3) Walter, M. G.; Warren, E. L.; McKone, J. R.; Boettcher, S. W.; Mi, Q.; Santori, E. A.; Lewis, N. S. Solar Water Splitting Cells. *Chem. Rev.* **2010**, *110*, 6446−6473.

(4) Lee, Y.; Suntivich, J.; May, K. J.; Perry, E. E.; Shao-Horn, Y. Synthesis and Activities of Rutile IrO2 and RuO2 Nanoparticles for Oxygen Evolution in Acid and Alkaline Solutions. *J. Phys. Chem. Lett.* **2012**, *3*, 399−404.

(5) Dau, H.; Limberg, C.; Reier, T.; Risch, M.; Roggan, S.; Strasser, P. The Mechanism of Water Oxidation: From Electrolysis via Homogeneous to Biological Catalysis. *ChemCatChem* **2010**, *2*, 724−761.

(6) Subbaraman, R.; Tripkovic, D.; Chang, K. C.; Strmcnik, D.; Paulikas, A. P.; Hirunsit, P.; Chan, M.; Greeley, J.; Stamenkovic, V.; Markovic, N. M. Trends in activity for the water electrolyser reactions on 3d M(Ni,Co,Fe,Mn) hydr(oxy)oxide catalysts. *Nat. Mater.* **2012**, *11*, 550−557.

(7) Pokhrel, R.; Goetz, M. K.; Shaner, S. E.; Wu, X.; Stahl, S. S. The "Best Catalyst" for Water Oxidation Depends on the Oxidation Method Employed: A Case Study of Manganese Oxides. *J. Am. Chem. Soc.* **2015**, *137*, 8384.

(8) Cheng, F.; Zhang, T.; Zhang, Y.; Du, J.; Han, X.; Chen, J. Enhancing electrocatalytic oxygen reduction on MnO(2) with vacancies. *Angew. Chem., Int. Ed.* **2013**, *52*, 2474−2477.

(9) Kuo, C.-H.; Mosa, M. I.; Poyraz, A. S.; Biswas, S.; El-Sawy, A. M.; Song, W.; Luo, Z.; Chen, S.-Y.; Rusling, J. F.; He, J.; Suib, S. L. Robust Mesoporous Manganese Oxide Catalysts for Water Oxidation. *ACS Catal.* **2015**, *5*, 1693.

(10) Jung, K.-N.; Riaz, A.; Lee, S.-B.; Lim, T.-H.; Park, S.-J.; Song, R.-H.; Yoon, S.; Shin, K.-H.; Lee, J.-W. Urchin-like a-MnO2 decorated with Au and Pd as a bi-functional catalyst for rechargeable lithium oxygen batteries. *J. Power Sources* **2013**, *244*, 328−335.

(11) Zaharieva, I.; Chernev, P.; Risch, M.; Klingan, K.; Kohlhoff, M.; Fischer, A.; Dau, H. Electrosynthesis, functional, and structural characterization of a water-oxidizing manganese oxide. *Energy Environ. Sci.* **2012**, *5*, 7081−7089.

(12) Miles, M. H.; Kissel, G.; Lu, P. W. T.; Srinivasan, S. Effect of Temperature on Electrode Kinetic Parameters for Hydrogen and Oxygen Evolution Reactions on Nickel Electrodes in Alkaline Solutions. *J. Electrochem. Soc.* **1976**, *123*, 332−336.

(13) Meng, Y.; Song, W.; Huang, H.; Ren, Z.; Chen, S. Y.; Suib, S. L. Structure-property relationship of bifunctional MnO2 nanostructures: highly efficient, ultra-stable electrochemical water oxidation and oxygen reduction reaction catalysts identified in alkaline media. *J. Am. Chem. Soc.* **2014**, *136*, 11452−64.

(14) Mohammad, A. M.; Awad, M. I.; El-Deab, M. S.; Okajima, T.; Ohsaka, T. Electrocatalysis by nanoparticles: Optimization of the loading level and operating pH for the oxygen evolution at crystallographically oriented manganese oxide nanorods modified electrodes. *Electrochim. Acta* **2008**, *53*, 4351−4358.

DOI: 10.1021/acssuschemeng.5b00324
ACS Sustainable Chem. Eng. 2015, 3, 2049−2057

(15) Boppana, V. B.; Jiao, F. Nanostructured MnO2: an efficient and robust water oxidation catalyst. *Chem. Commun.* **2011**, *47*, 8973−8975.
(16) Date, M.; Haruta, M. Moisture effect on CO oxidation over Au/TiO2 catalyst. *J. Catal.* **2001**, *201*, 221−224.
(17) Jiang, F.; Zhu, X.; Fu, B.; Huang, J.; Xiao, G. Au/γ-MnO2 catalyst for solvent-free toluene oxidation with oxygen. *Chin. J. Catal.* **2013**, *34*, 1683−1689.
(18) Ye, Q.; Zhao, J.; Huo, F.; Wang, D.; Cheng, S.; Kang, T.; Dai, H. Nanosized Au supported on three-dimensionally ordered mesoporous β-MnO2: Highly active catalysts for the low-temperature oxidation of carbon monoxide, benzene, and toluene. *Microporous Mesoporous Mater.* **2013**, *172*, 20−29.
(19) Alhumaimess, M.; Lin, Z.; He, Q.; Lu, L.; Dimitratos, N.; Dummer, N. F.; Conte, M.; Taylor, S. H.; Bartley, J. K.; Kiely, C. J.; Hutchings, G. J. Oxidation of benzyl alcohol and carbon monoxide using gold nanoparticles supported on MnO2 nanowire microspheres. *Chem. - Eur. J.* **2014**, *20*, 1701−10.
(20) Liu, X. J.; Liu, J. F.; Li, Y. P.; Li, Y. J.; Sun, X. M. Au/NiCo2O4 Arrays with High Activity for Water Oxidation. *ChemCatChem* **2014**, *6*, 2501−2506.
(21) Gorlin, Y.; Chung, C.-J.; Benck, J. D.; Nordlund, D.; Seitz, L.; Weng, T.-C.; Sokaras, D.; Clemens, B. M.; Jaramillo, T. F. Understanding Interactions between Manganese Oxide and Gold That Lead to Enhanced Activity for Electrocatalytic Water Oxidation. *J. Am. Chem. Soc.* **2014**, *136*, 4920−4926.
(22) Frydendal, R.; Busch, M.; Halck, N. B.; Paoli, E. A.; Krtil, P.; Chorkendorff, I.; Rossmeisl, J. Enhancing Activity for the Oxygen Evolution Reaction: The Beneficial Interaction of Gold with Manganese and Cobalt Oxides. *ChemCatChem* **2015**, *7*, 149−154.
(23) Padayachee, D.; Golovko, V.; Marshall, A. T. The effect of MnO2 loading on the glycerol electrooxidation activity of Au/MnO2/C catalysts. *Electrochim. Acta* **2013**, *98*, 208−217.
(24) Li, X.; Liu, J.; Zhao, Y.; Zhang, H.; Du, F.; Lin, C.; Zhao, T.; Sun, Y. Significance of surface trivalent manganese in electro-catalytic activity of water oxidation in undoped and doped MnO_2 nanowires. *ChemCatChem* **2015**, *7*, 1848−1856.
(25) Wang, X.; Li, Y. Synthesis and formation mechanism of manganese dioxide nanowires/nanorods. *Chem. - Eur. J.* **2003**, *9*, 300−306.
(26) Zhou, X. L.; Wei, Q. M.; Sun, K.; Wang, L. M. Formation of ultrafine uniform gold nanoparticles by sputtering and redeposition. *Appl. Phys. Lett.* **2009**, *94*, 133107-1−133107-7.
(27) Reznickova, A.; Novotna, Z.; Kasalkova, N. S.; Svorcik, V. Gold nanoparticles deposited on glass: physicochemical characterization and cytocompatibility. *Nanoscale Res. Lett.* **2013**, *8*, 252.
(28) Wang, L.-C.; Liu, Y.-M.; Chen, M.; Cao, Y.; He; Fan, K.-N. MnO2 Nanorod Supported Gold Nanoparticles with Enhanced Activity for Solvent-free Aerobic Alcohol Oxidation. *J. Phys. Chem. C* **2008**, *112*, 6981−6987.
(29) Zanella, R.; Giorgio, S.; Henry, C. R.; Louis, C. Alternative Methods for the Preparation of Gold Nanoparticles Supported on TiO2. *J. Phys. Chem. B* **2002**, *106*, 7634−7642.
(30) Wang, X.; Sun, S.; Huang, Z.; Zhang, H.; Zhang, S. Preparation and catalytic activity of PVP-protected Au/Ni bimetallic nanoparticles for hydrogen generation from hydrolysis of basic NaBH4 solution. *Int. J. Hydrogen Energy* **2014**, *39*, 905−916.
(31) Behrisch, R. *Sputtering by Particle bombardment*; Springer: Berlin, 1991.
(32) Longo, L. F. L.; Carlo, G. Di; Giannici, F.; Venezia, A. M.; Martorana, A. Structure and the Metal Support Interaction of the Au/Mn Oxide Catalysts. *Chem. Mater.* **2010**, *22*, 3952−3960.
(33) Lai, Y.; Li, Y.; Jiang, L.; Xu, W.; Lv, X.; Li, J.; Liu, Y. Electrochemical behaviors of co-deposited Pb/Pb−MnO2 composite anode in sulfuric acid solution − Tafel and EIS investigations. *J. Electroanal. Chem.* **2012**, *671*, 16−23.
(34) Shimizu, T.; Okushi, H. Intrinsic electrical properties of Au/$SrTiO_3$ Schottky junctions. *J. Appl. Phys.* **1999**, *85*, 7244−7251.
(35) Das, S. N.; Choi, J. H.; Kar, J. P.; Moon, K. J.; Il Lee, T.; Myoung, J. M. Junction properties of Au/ZnO single nanowire Schottky diode. *Appl. Phys. Lett.* **2010**, *96*, 092111−092111-3.
(36) Liu, S.; Hu, F.; Zhang, J.; Tang, H.; Shao, M. Surface-doping effect of InVO4 nanoribbons and the distinctive behavior as gas sensors. *ACS Appl. Mater. Interfaces* **2013**, *5*, 3208−3211.
(37) Li, X.; Xiao, Y.; Zhou, K.; Wang, J.; Schweizer, S. L.; Sprafke, A.; Lee, J. H.; Wehrspohn, R. B. Photoelectrochemical hydrogen evolution of tapered silicon nanowires. *Phys. Chem. Chem. Phys.* **2015**, *17*, 800−804.
(38) Meng, Y.; Song, W.; Huang, H.; Ren, Z.; Chen, S. Y.; Suib, S. L. Structure-property relationship of bifunctional MnO2 nanostructures: highly efficient, ultra-stable electrochemical water oxidation and oxygen reduction reaction catalysts identified in alkaline media. *J. Am. Chem. Soc.* **2014**, *136*, 11452−11464.
(39) Park, J.; Kim, H.; Jin, K.; Lee, B. J.; Park, Y.-S.; Kim, H.; Park, I.; Yang, K. D.; Jeong, H.-Y.; Kim, J.; Hong, K. T.; Jang, H. W.; Kang, K.; Nam, K. T. A New Water Oxidation Catalyst: Lithium Manganese Pyrophosphate with Tunable Mn Valency. *J. Am. Chem. Soc.* **2014**, *136*, 4201−4211.
(40) Dicastro, V.; Polzonetti, G. XPS Study of MnO Oxidation. *J. Electron Spectrosc. Relat. Phenom.* **1989**, *48*, 117−123.
(41) Schilling, O.; Dahn, J. R. Fits of the γ-MnO2 Structure Model to Disordered Manganese Dioxides. *J. Appl. Crystallogr.* **1998**, *31*, 396−406.
(42) Park, J.; Kim, H.; Jin, K.; Lee, B. J.; Park, Y. S.; Kim, H.; Park, I.; Yang, K. D.; Jeong, H. Y.; Kim, J.; Hong, K. T.; Jang, H. W.; Kang, K.; Nam, K. T. A New Water Oxidation Catalyst: Lithium Manganese Pyrophosphate with Tunable Mn Valency. *J. Am. Chem. Soc.* **2014**, *136*, 4201−4211.
(43) Gao, T.; Norby, P.; Krumeich, F.; Okamoto, H.; Nesper, R.; Fjellvåg, H. Synthesis and Properties of Layered-Structured Mn5O8Nanorods. *J. Phys. Chem. C* **2010**, *114*, 922−928.
(44) Kuo, C. H.; Li, W.; Pahalagedara, L.; El-Sawy, A. M.; Kriz, D.; Genz, N.; Guild, C.; Ressler, T.; Suib, S. L.; He, J. Understanding the role of gold nanoparticles in enhancing the catalytic activity of manganese oxides in water oxidation reactions. *Angew. Chem., Int. Ed.* **2015**, *54*, 2345−2350.
(45) Takashima, T.; Hashimoto, K.; Nakamura, R. Mechanisms of pH-dependent activity for water oxidation to molecular oxygen by MnO2 electrocatalysts. *J. Am. Chem. Soc.* **2012**, *134*, 1519−1527.

DOI: 10.1021/acssuschemeng.5b00324
ACS Sustainable Chem. Eng. 2015, 3, 2049−2057